

Giant Concentric Metallo-Supramolecule with Aggregation-Induced Phosphorescent Emission

Yiming Li^{†,∇,‡}, Gui-Fei Huo[‡], Bingqing Liu[‡], Bo Song^{//}, Yuan Zhang[§], Xiaomin Qian[∇], Heng Wang[†], Guang-Qiang Yin[†], Alexander Filosa[∇], Wenfang Sun[‡], Saw Wai Hla[#], Hai-Bo Yang[‡] and Xiaopeng Li^{†,*}

[†] College of Chemistry and Environmental Engineering, Shenzhen University, Shenzhen, 518055, China

[∇] Department of Chemistry, University of South Florida, Tampa, FL, 33620, USA

[‡] Shanghai Key Laboratory of Green Chemistry and Chemical Processes, Department of Chemistry, East China Normal University, Shanghai, 200062, China

[‡] Department of Chemistry and Biochemistry, North Dakota State University, Fargo, ND, 58105, USA

^{//} Department of Chemistry, Northwestern University, Evanston, IL, 60208, USA

[§] Department of Physics, Old Dominion University, Norfolk, VA, 23529, USA

[#] Nanoscience and Technology Division, Argonne National Laboratory, Lemont, IL, 60439, USA

KEYWORDS. Aggregation-Induced Emission, Metallo-Supramolecule, Phosphorescence, Self-Assembly, Terpyridine

ABSTRACT: Fluorescent metallo-supramolecules have received considerable attention due to their precisely-controlled dimensions as well as the tunable photophysical and photochemical properties. However, phosphorescent analogues are still rare, and limited to small structures with low-temperature phosphorescence. Herein, we report the self-assembly and photophysical studies of a giant, discrete metallo-supramolecular concentric hexagon functionalized with six alkynylplatinum(II) bzimpy moieties. With a size larger than 10 nm and molecular weight higher than 26,000 Da, the assembled terpyridine-based supramolecule displayed phosphorescent emission at room temperature. Moreover, the supramolecule exhibited enhanced aggregation-induced phosphorescent emission compared to the ligand by tuning the aggregation states through intermolecular interactions, and significant enhancement of emission to CO₂ gas.

Introduction

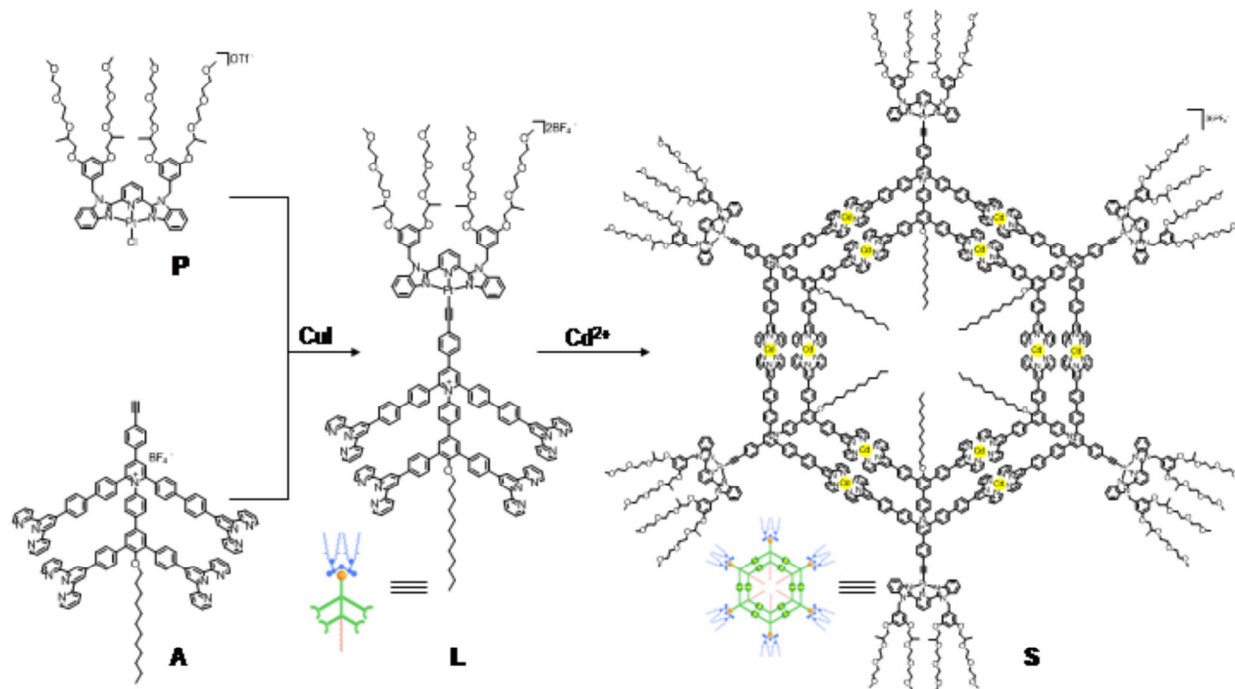
Discrete metallo-supramolecules obtained via coordination-driven self-assembly have emerged as a class of materials to bridge the gap between small molecules and polymers,¹ on account of the precisely-controlled dimensions that provide an ideal platform for investigations of structure-property-function relationships.² Among the various functions, the luminescence of metallo-supramolecules has a wide range of applications in sensing,³ photocatalysis,⁴ bioimaging,⁵ light-harvesting,⁶ phototherapy⁷ and so on.⁸ Emissive metallo-supramolecules have been constructed mainly through the following three strategies: (i) introducing the luminophores into the scaffolds;⁹ (ii) attaching the luminophores on the backbone as accessories;^{7c, 10} (iii) encapsulating luminophores in the cavity of the structures through host-guest chemistry.^{8f, 11} Generally, the luminophores include small organic motifs, such as tetraphenylethylene,¹² boron-dipyrromethene (BODIPY),^{5b, 13} triphenylamine,¹⁴ pyrene,¹⁵ and perylene diimide,¹⁶ as well as emissive metal complexes containing Ru(II),¹⁷ Eu(III),¹⁸ Ir(III),^{6a, 10, 19} Pt(II),²⁰ and Au(I).²¹ Among these emissive metallo-supramolecules, however, phosphorescent analogues are still rare, and mainly limited to small structures with low-temperature phosphorescence.^{18d, 20a, 21a, 22}

2,2':6',2''-terpyridine (tpy) as one of the most intensively investigated building blocks, has been widely used in constructing sophisticated metallo-supramolecular architectures with well-defined sizes, shapes and geometries.²³ With weak luminescence, tpy has been functionalized with many luminophores to tune the emissive properties of corresponding metal complexes.²⁴ For instance, Cd(II) was frequently assembled with tpy to construct fluorescent supramolecules,²⁵ among which characteristic aggregation-induced emission (AIE)^{12a, 26} was observed. Recent examples further employed tpy building blocks to construct phosphorescent metallo-polymers.²⁷ Among the luminophores, square-planar Pt(II) motifs have received considerable attention because of their unique photophysical and electrochemical properties.²⁸ These complexes exhibit phosphorescence brought by the heavy-atom effect with tunable emission wavelengths and lifetimes.^{28b, 29} Also, Pt(II) luminophores are prone to have strong intermolecular Pt...Pt interaction,³⁰ which can manipulate their aggregations and enable emission through aggregation-induced phosphorescent emission (AIPE) effect,³¹ a variant of AIE. More importantly, Pt(II) complexes are thermodynamically stable and kinetically inert.^{28a} Thus, such features facilitate the synthesis

of tpy building blocks with Pt(II) luminophores for further

coordination-driven

self-assembly.



Scheme 1. Synthesis of ligand **L** and self-assembly of metallo-supramolecule **S**.

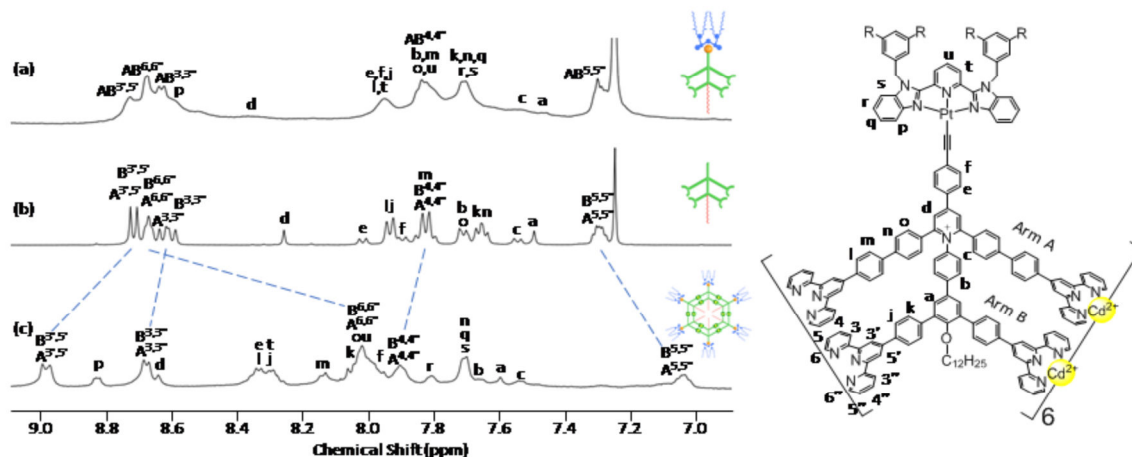


Figure 1. ^1H NMR spectra of (a) **L** in CDCl_3 (b) **A** in CDCl_3 , and (c) **S** in CD_3CN . The broad signals of **L** were attributed to the strong aggregation in solution.

On the basis of previous study, we speculated the combination of AIPE-active Pt(II) components with tpy-based emissive supramolecules could create a synergy, by which the emissive properties of individual components could be retained, and the hybrid supramolecular architectures could even display superior AIPE compared to the individual components. According to this speculation, we designed a giant but discrete metallo-supramolecular concentric hexagon (**S**) functionalized with six Pt(II) bzimpy (bzimpy=2,6-bis(benzimidazole-2'-yl)pyridine) motifs. In the design, a terminal alkynyl group was employed to install the Pt(II) motif with a stable and rigid Pt(II)-alkynyl bond for further self-assembly. Also, we introduced multiple hydrophilic ethylene glycol chains into bzimpy moieties on the periphery, and long alkyl chain (C_{12}) into the interior to tune the aggregation through balancing the overall hydrophobicity/hydrophilicity. With a size larger than 10 nm and a molecular weight higher than 26,000 Da, the assembled

tpy-based supramolecule containing six Pt(II) centers displayed phosphorescent emission with a lifetime of 218 ns at room temperature. By synergistically combining AIPE from Pt(II) luminophores and AIE features from Cd(II)-tpy assemblies, the functionalized supramolecule **S** exhibited significantly enhanced AIPE compared to the ligand **L**. Via tuning the aggregation states of the functionalized ligand **L** and **S**, their AIPE behaviors were carefully investigated. More interestingly, further enhancement of phosphorescent emission was observed in both **L** and **S** when purged by CO_2 gas. As such, this system is expected to find practical applications, such as gas sensing.

Results and Discussion

In the synthesis of building block **L**, tetratopic tpy-pyridinium salt precursor **A** was synthesized using a modified procedure as previously reported.^{23h} A terminal alkynyl group

was introduced into the backbone of **A** in order to further functionalize the metallo-supramolecule, including the installation of the following Pt(II) motif with the stable and rigid Pt(II)-alkynyl bond. The detailed synthesis procedure for **A** and chloroplatinum(II) bzimpy precursor **P** (Scheme S1) is described in the Supporting Information (SI). The final alkyneplatinum(II) bzimpy ligand **L** was synthesized by bridging **P** and **A** in the presence of a catalytic amount of copper(I) iodide and triethylamine in DMF solution under N_2 atmosphere.

All of the ligand and precursors were fully characterized by multi-dimensional nuclear magnetic resonance (NMR), including 1H , ^{13}C , 2D correlation spectroscopy (2D COSY), and/or Nuclear Overhauser Effect Spectroscopy (NOESY), as well as electrospray ionization mass spectrometry (ESI-MS) (See details in SI). It is noteworthy that the proton resonance of ligand **L** showed very broad signals in $CDCl_3$ (Figure 1a), as well as in CD_3CN (Figure S38). In contrast, the proton resonance for the Pt(II) free precursor **A** displayed sharp signals (Figure 1b). All these results suggested that **L** was highly prone to aggregate in solutions through intermolecular Pt \cdots Pt and π - π interactions³².

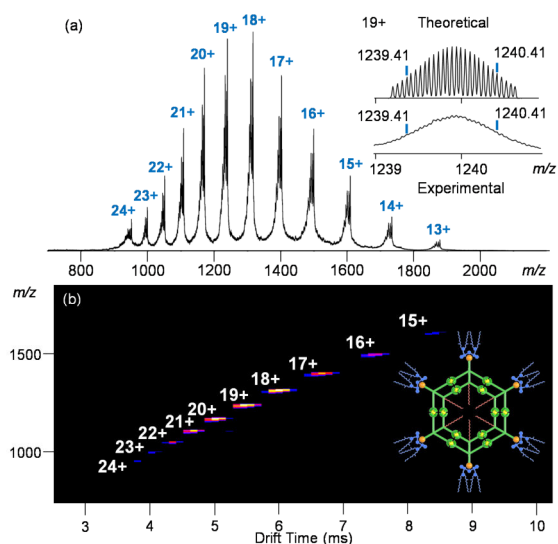


Figure 2. (a) ESI-MS and (b) TWIM-MS plots of **S**.

The self-assembly of **S** was achieved by treating **L** with $Cd(NO_3)_2$ in a stoichiometric ratio of 1:2, followed by counterion exchange with excess NH_4PF_6 to give **S** as a yellow precipitate in a high yield. The 1H NMR spectrum of the supramolecule (Figure 1c) showed much sharper signals compared with the spectrum of **L**, indicating weaker aggregation of **S** owing to the bulky size of the octahedral coordination of $<tpy-Cd(II)-tpy>$ unit that reduced the intermolecular Pt \cdots Pt interactions. Two characteristic singlets with an integration ratio of 1:1 were observed at 9.00 ppm and 8.97 ppm, respectively, which were assigned to the tpy- $H^{3,5'}$ protons of the inner and outer layer, excluding the formation of polymeric species. Compared with those of **A**, the tpy- $H^{3,5'}$ signals of **S** showed a diagnostic downfield shifted (*ca.* 0.3 ppm), while the tpy- $H^{6,6'}$ peaks exhibited a significantly upfield shift (*ca.* 0.7 ppm), indicating the complexation of tpy units with Cd(II). Diffusion Ordered Spectroscopy (DOSY) NMR of **S** revealed a narrow band with diffusion coefficient $\log D = -9.20$ at 298 K (Figure

S50), suggesting the formation of a discrete structure. All the assignments were further supported by 2D COSY and NOESY spectra (Figures S45-S49).

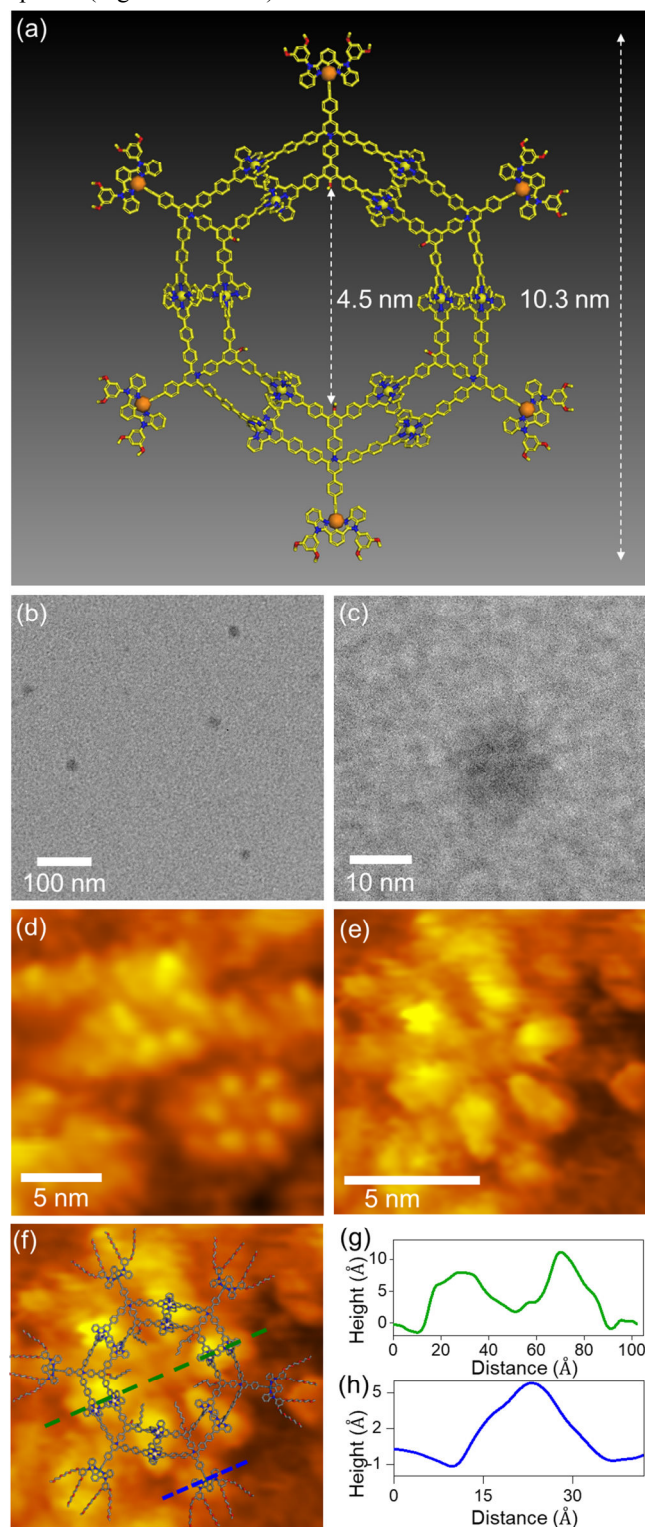


Figure 3. TEM and STM imaging of **S**. (a) Molecular modeling of **S** (Ethylene glycol and alkyl chains were omitted for clarity.) (b) TEM image of **S**. (c) Magnified TEM image of **S**. (d) A large area STM image of **S** showing the presence of two supramolecules. [Imaging parameters: $V_t = 2.5$ V, and $I_t = 35$ pA]. (e) Magnified image of a single supramolecule. (f) STM image of **S** with molecular modeling overlay [Imaging param-

eters: $V_t = 2.5$ V, and $I_t = 29$ pA]. (g and h) STM line profiling measurements made along the green and blue dashed lines shown in (f).

In addition, electrospray ionization-mass spectrometry (ESI-MS) and traveling wave ion mobility-mass spectrometry (TWIM-MS)³³ were used to characterize the functionalized supramolecule. A series of peaks with continuous charges from 13+ to 24+ was observed in ESI-MS (Figure 2a), due to the successive loss of PF_6^- counterions. After deconvolution, the molecular weight was calculated as 26,301 Da, corresponding to the chemical composition of $\text{C}_{1188}\text{H}_{1152}\text{N}_{108}\text{O}_{102}\text{Pt}_6\text{Cd}_{12}\text{P}_{36}\text{F}_{216}$. The experimental isotope pattern of each charge state agreed well with the corresponding simulated peak (Figure 2a inset, Figure S63). Moreover, only one set of signals was observed from TWIM-MS, indicating that there was no other structural conformer or isomer for the assembled structure (Figure 2b).

To further study the structure of the supramolecule, transmission electron microscope (TEM) was utilized to verify the size and shape of **S**. The supramolecules were observed as a dispersion of individual uniform dots (Figure 3b). The average size of the particles was in good agreement with the theoretical diameter calculated by molecular modeling (Figure 3a and c). In order to directly visualize the structure of the metallo-supramolecules with high resolution, ultrahigh vacuum-low temperature-scanning tunneling microscope (UHV-LT-STM) was also applied.^{23k, 34} Ultrahigh vacuum provided a clean and neat environment to minimize noise, and low temperature would reduce thermal motion, thus leading to a higher resolution. A very dilute solution of **S** was drop-casted on a Ag(111) substrate followed by cooling down to 4 K. Due to the octahedral coordination and high electron density around the metal center, the STM imaging showed six elliptic bright dots corresponding to <tpy-Cd(II)-tpy> units, which depicted the framework of hexagonal structure (Figure 3d-f). Within the magnified image, the shape and direction of each elliptic-shaped lobe can be distinctly observed. Note that each dot was attributed as the fusion of signals from two <tpy-Cd(II)-tpy> units in the two layers because of the short distance between them. Moreover, the double-layered scaffold without Pt(II) motifs was measured to have a diameter of ~8 nm and a height of ~10 Å (Figure 3f-h), which agreed well with the theoretical modeling (Figure 3a). In sharp contrast to the bright lobes of <tpy-Cd(II)-tpy> units in STM measurement, Pt atoms did not exhibit strong signals. We speculated that the bulky <tpy-Cd(II)-tpy> unit with octahedral coordination geometry might lift the entire organic moieties off the substrate, as well as the end groups of alkyne-Pt bzimpy. Therefore, the square planer Pt(II) center could have less contact with the surface, leading to the loss of tunneling current.

After the structural characterization, the emission properties of **S**, **L** and the precursors **A** and **P** were investigated in acetonitrile solutions (mixed with 5% CH_2Cl_2 for **A**) at room temperature. The normalized emission spectra are shown in Figure 4a and the emission parameters, including emission wavelengths and lifetimes are listed in Table S1. The emissions of **P**, **L**, and **S** exhibited large Stokes shifts (> 200 nm) with respect to their corresponding absorption bands (Figure S64),³⁵ and were prone to oxygen quenching. Additionally, the recorded emission lifetimes of **L** and **S** deduced from the decay traces were 270 and 218 ns, respectively (Figure 4b and c) which are longer than those of general fluorescence. These

features implied a nature of room-temperature phosphorescence through the emission from the triplet excited states.

The emission spectra of **P**, **L**, and **S** resembled each other with essentially the same energy and similar vibronic progressions, indicating the same/similar original emitting excited states. The vibronic spacing between the band maxima (*ca.* 567 nm) and the shoulder (*ca.* 606 nm) was approximately 1135 cm^{-1} , which is in accordance with the stretching mode of the aromatic rings.³⁵ Also, broad tails were observed in **L** and **S** compared to **P** due to the metal-metal-to-ligand charge transfer (³MMLCT) excited states from the $\text{Pt}\cdots\text{Pt}$ and π - π stacking interactions.³² In view of the similar structural component in these three complexes, *i.e.*, bzimpy, as similar $[(\text{N}^{\wedge}\text{N}^{\wedge}\text{N})\text{PtCl}]^+$ complex reported in the literature, we attribute the observed emission originating from the metal-perturbed ³ π,π^* emission of the bzimpy.³⁶ Pt(II)-contained precursor **P** exhibited short-lived emission of 18 ns (Figure S65). This phenomenon could be ascribed to the presence of thermally accessible low-lying metal-centered non-emissive ³ d,d state, which provided an additional decay pathway and quenched the ligand-localized ³ π,π^* emission. This is a common feature in many other $[(\text{N}^{\wedge}\text{N}^{\wedge}\text{N})\text{PtCl}]^+$ complexes.³⁷ When the Cl ligand in **P** was replaced by the acetylide ligand in **L**, the electron-donating ability of the acetylide ligand lifted up the ³ d,d state with a negligible impact on the energy of the ³ π,π^* state. This separated the non-emissive ³ d,d state from the emitting ³ π,π^* state further, and consequently improved the emission in **L**. The introduction of heavy-atom Cd(II) during the self-assembly of **L** into **S** could induce intersystem crossing (a competing nonradiative thermal process with the radiative decay path) from the T_1 to S_0 . Meanwhile, the weak ligand field strength of Cd(II) ion would narrow the energy gap between the nonemissive ³ d,d state and the emitting ³ π,π^* state, which would decrease the lifetime of **S**. Interestingly, **S** still retained a relatively long lifetime of 218 ns. It is worth noting that these phosphorescent properties are quite unique for such a giant supramolecule with a diameter of 10 nm.

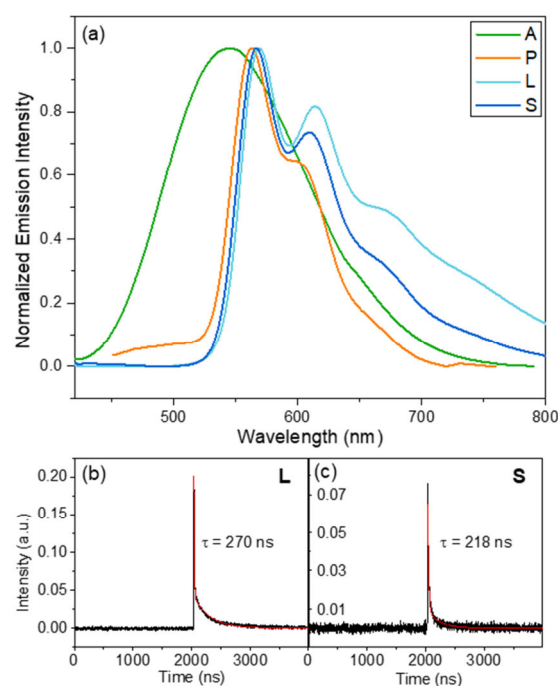


Figure 4. (a) Normalized emission spectra of **P** and **A** ($\lambda_{\text{ex}} = 390 \text{ nm}$), **L** and **S** ($\lambda_{\text{ex}} = 370 \text{ nm}$) in N_2 deoxygenated acetonitrile

(with 5% CH_2Cl_2 for **A**) at room temperature ($c = 1 \times 10^{-5} \text{ mol/L}$). Emission lifetime decay traces of (b) **L** and (c) **S**.

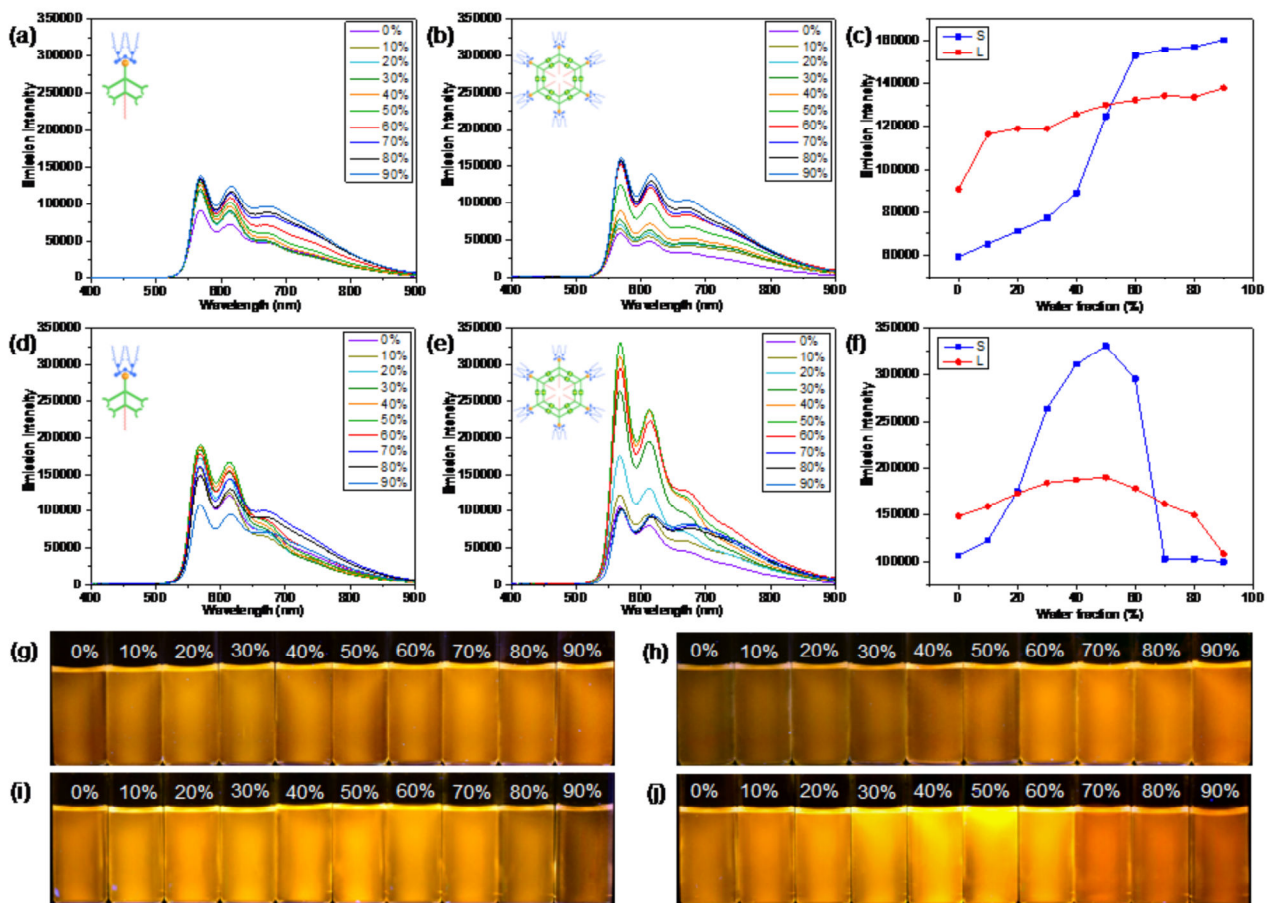


Figure 5. Emission spectra of **L** and **S**. (a) Emission spectra of ligand **L** in non-deoxygenated acetonitrile/water solvent ($\lambda_{\text{ex}} = 370 \text{ nm}$, $c = 3.5 \mu\text{M}$). (b) Emission spectra of **S** in non-deoxygenated acetonitrile/water solvent ($\lambda_{\text{ex}} = 370 \text{ nm}$, $c = 0.6 \mu\text{M}$). (c) Emission intensity of **L** and **S** at 567 nm with different fraction of water in non-deoxygenated acetonitrile/water solution (d) Phosphorescent emission spectra of **L** with N_2 deoxygenated acetonitrile/water solvent ($\lambda_{\text{ex}} = 370 \text{ nm}$, $c = 3.5 \mu\text{M}$). (e) Phosphorescent emission spectra of **S** with N_2 deoxygenated acetonitrile/water solvent ($\lambda_{\text{ex}} = 370 \text{ nm}$, $c = 0.6 \mu\text{M}$). (f) Emission intensity of **L** and **S** at 567 nm with different fraction of water in N_2 deoxygenated acetonitrile/water solution. (g) Emission photographs of **L** in non-deoxygenated acetonitrile/water with various water fractions. (h) Emission photographs of **S** in non-deoxygenated acetonitrile/water with various water fractions. (i) Emission photographs of **L** in N_2 deoxygenated acetonitrile/water with various water fractions (under 365 nm UV lamp). (j) Emission photographs of **S** in N_2 deoxygenated acetonitrile/water with various water fractions (under 365 nm UV lamp).

To investigate the intermolecular interactions within ligands and supramolecules, temperature-dependent emission studies were performed (Figure S66). The spectra of both **L** and **S** showed that with the elevation of the temperature, the intensity of the emission decreased dramatically as the non-covalent interactions could become negligible at high temperature.³⁸ These results suggested the existence of $\text{Pt} \cdots \text{Pt}$ interactions in both ligand **L** and supramolecule **S** at room temperature. Indeed, the formation of aggregations by $\text{Pt} \cdots \text{Pt}$ interactions brought the restriction of intramolecular rotation (RIR) effect at low temperature^{26d, 26e}, and immobilized the luminophores on the molecules, leading to the enhancement of emission.

Further detailed photophysical studies of **L** and **S** were performed in acetonitrile/water mixed solvents with various fractions of poor solvent (i.e., water), to investigate the AIPE effects. Since both **L** and **S** have installed multiple ethylene glycol chains for enhanced solubility in aqueous solutions, they

did not show immediate precipitation with high fraction of water. When the fraction of water was increased, the UV-vis absorption spectra of both **L** and **S** (Figure S67) displayed a rise in the absorption tail around 480 nm, indicating the growth of ³MMLCT transition due to $\text{Pt} \cdots \text{Pt}$ interaction^{30d, 39}

Both the ligand **L** and the supramolecule **S** showed weak emission in pure acetonitrile, with increasing the fraction of water as the poor solvent, **S** exhibited stronger emission in its aggregation state due to the cooperative effect from Pt(II) motif and $\langle \text{tpy-Cd(II)-tpy} \rangle$ units (Figure 5a and b). Furthermore, in the deoxygenated solvent without oxygen-quenching for the phosphorescence, supramolecule **S** exhibited significantly enhanced AIPE compared to ligand **L**, i.e., the maximum in emission intensity reached 3.1-fold enhancement for **S** but only 1.3-fold increase for **L** (Figure 5b and 5e). In addition, the AIPE behavior was well maintained along with the increasing fraction of water from 0% to 50%. However, further

increasing the poor solvent fraction (60% to 90%) resulted in a decrease of phosphorescent intensity. Due to the poor solubility of **L** and **S** in water, we observed large aggregates formed

in the solutions with high water fractions after the deoxygenating process.

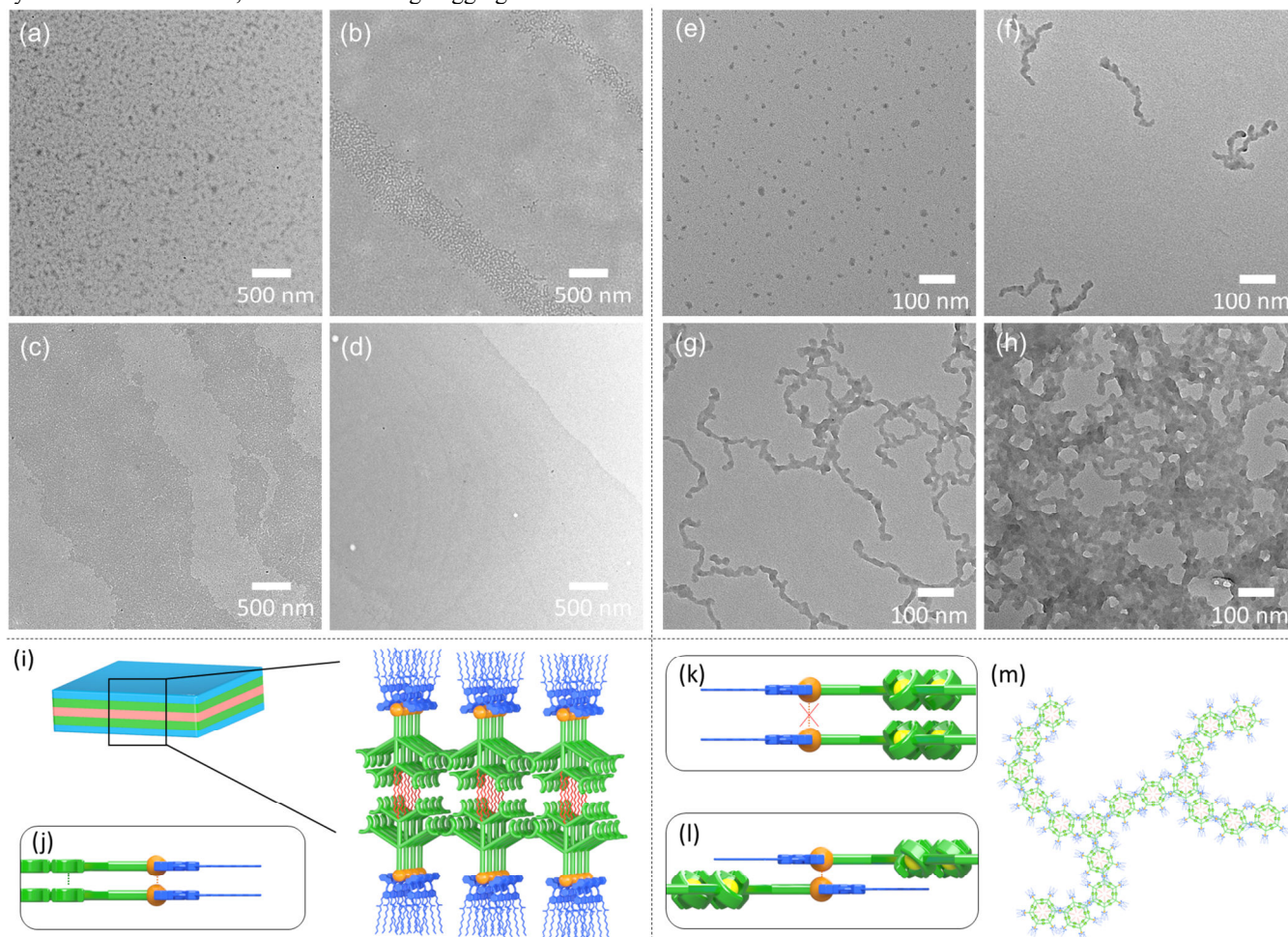


Figure 6. TEM images of **L** and **S** aggregates. TEM images of the aggregates of **L** formed in acetonitrile/water mixtures containing (a) 20%, (b) 40%, (c) 60%, and (d) 80% water, and aggregates of **S** formed in acetonitrile/water mixtures containing (e) 20%, (f) 40%, (g) 60%, and (h) 80% water. (i) Proposed formation of sheet-like aggregates by **L**. (j) Proposed Pt···Pt interaction and π - π stacking between ligands with face-to-face direction. (m) Worm-like aggregates of **S**. (k) Unfavourable face-to-face stacking. (l) Proposed head-to-tail Pt···Pt interaction bridging supramolecules without ring stacking.

And the precipitation formation caused the decrement of phosphorescent intensity.

For further comparison and investigation of the AIPE mechanism, supramolecule **C** without Pt(II) motif was constructed (see detailed characterizations in Figures S39-S44, S61 and S62) by assembling **A** and Cd(II) directly (Scheme S4). The emission enhancement was also observed by increasing the fraction of water (Figure S69a), suggesting the AIE feature of Cd(II)-tpy based supramolecules. However, **C** exhibited short-lived emission less than 5 ns and no further enhancements were observed with deoxygenated solvent (Figure S69b), indicating that this emission was fluorescence only.

Interestingly, variations in emission spectra were observed by using different gases to deoxygenate the solvent (Figure S70). It was found that CO₂ can further trigger substantial enhancements in emission intensity compared with the results in non-deoxygenated solvent (*ca.* 5.5-fold increase in case of **S**, and 1.8-fold increase in case of **L**). As a comparison, N₂ brought weaker enhancement for **L** and **S**, *i.e.*, 3.3- and 1.3-fold increase, respectively. We speculated that CO₂ might have weak interactions with Pt(II)⁴⁰, since CO₂ has a kinetic

diameter of 3.3 Å, which is very close to the ideal distance between Pt atoms in Pt···Pt interaction (3.5 Å). As such, CO₂ might strengthen the Pt···Pt interactions between supramolecules with a higher RIR effect, leading to an increased emission. In addition, **S** exhibited more significant responses to different gases than **L**, perhaps due to the cooperative effect of multiple Pt(II) centers within the large supramolecular architectures. This property may lead to a potential application for gas sensing⁴¹.

Morphology studies of aggregates were generally used for evaluating aggregation behaviors and investigating AIE or AIPE mechanism. Dynamic light scattering (DLS) and TEM were utilized to further elucidate the relationship between luminescent properties and aggregation of the ligand **L** and supramolecule **S**. The DLS results (Figure S71) showed the average hydrodynamic diameters (D_h) of the aggregations of **L** and **S** were increased with the increment of the water fraction. Also, the TEM images (Figure 6a-6d) showed that **L** aggregated into layered nanosheet structure in acetonitrile/water, and the size of the sheet was increased with the increment of water portion. In contrast, **S** aggregated into worm-like structures

(Figure 6e-6h). With the increase of the water fraction, the length of the worm-like aggregates extended and finally became a cross-linked structure. These results agreed well with the AIPE effect observed in acetonitrile/ water solvent.

It is interesting to observe the tremendously different aggregation morphologies of **L** and **S**. To further gain insight of the aggregation mechanism, different solvent mixtures were used to investigate their aggregation behaviors. Comparing with the layered structure observed in CH₃CN/water system, **L** formed spherical aggregates with diameters around 100 nm in DMF/Et₂O solution, and larger spherical structures could be observed in DMF/*i*-Pr₂O system (Figure S72). The difference between the sheet and sphere is possibly due to the long hydrophobic/hydrophilic chains decorated on the inner and outer rims of the ligand performing differently in aqueous/nonaqueous solutions. According to the observation, we postulated that both Pt···Pt interaction and π - π stacking might work simultaneously to organize ligand **L** with a face-to-face direction (Figure 6j).

In a sharp contrast, after coordinating with Cd(II), the metallo-supramolecule **S** did not aggregate into spherical/layered morphologies as **L**, or a tubular structure as the unfunctionalized concentric hexagons.^{23h} Instead, the amorphous worm-like structure was the only morphology observed in several different solvent systems (Figure S73). We speculated that the entire concentric hexagon core played an essential role in regulating the aggregating behavior of Pt-Pt interaction and determining the final morphology of the hierarchical self-assembly. Since the ideal distance between Pt atoms in Pt···Pt interaction is reported around 3.5 Å,⁴² the bulky octahedral coordination of <tpy-Cd(II)-tpy> with height of 10 Å as measured from STM can effectively prohibit the formation of π - π stacking and block the Pt-Pt interaction from face-to-face orientation (Figure 6k), but force the Pt-Pt interaction to a head-to-tail way (Figure 6l). The emissive behavior of individual components (Pt and tpy) was retained in supramolecule **S**, which even displayed enhanced phosphorescent properties during aggregation than individual components.

Conclusions

In summary, a giant but discrete concentric metallo-supramolecule with six well-arrayed alkynyl-platinum(II) bzimpy groups was assembled through rational design to enrich the library of phosphorescent metallo-supramolecules, which still remain in the infancy. The cyclic structure was clearly visualized by STM imaging at the submolecular resolution. With the Pt(II) motifs installed, functionalized ligand and metallo-supramolecule exhibited room-temperature phosphorescence with lifetimes of 270 ns and 218 ns, respectively. With the AIE enhancement from the <tpy-Cd(II)-tpy> coordination, supramolecule **S** exhibited conspicuously stronger AIPE compared to ligand **L**. In addition, both ligand and supramolecule exhibited significant responses to CO₂ gas, indicating the potential existence of weak interaction between gas molecules and aggregates. Regarding the aggregation behaviors driven by intermolecular interactions, the ligand could aggregate into layered and spherical structures in different solvent systems, while the supramolecule could only aggregate into worm-like structure and gel at high concentration. Our endeavors expand the scope of discrete phosphorescent materials into the dimensions beyond 10 nm, and will shed lights

on the development of novel phosphorescent materials that combine the advantages from small molecules and polymers, i.e., precise functions, high level of sophistication and facile device fabrication.

ASSOCIATED CONTENT

Supporting Information

Synthetic details, ligands and complexes characterization including ¹H NMR, ¹³C NMR, 2D COSY, 2D NOESY, ESI-MS, TWIM-MS, UV-Vis, TEM are included in supporting information. The Supporting Information is available free of charge on the ACS Publications website.

AUTHOR INFORMATION

Corresponding Author

xiaopengli@szu.edu.cn

Author Contributions

‡ Y.L. and G.-F. H. contributed equally.

Notes

The authors declare no competing financial interests.

ACKNOWLEDGMENT

This research was supported by Shenzhen University and University of South Florida. Use of the Center for Nanoscale Materials, an Office of Science user facility, was supported by the U.S. Department of Energy, Office of Science, Office of Basic Energy Sciences, under Contract No. DE-AC02-06CH11357.

REFERENCES

- (1). (a) Ruben, M.; Rojo, J.; Romero-Salguero, F. J.; Uppadine, L. H.; Lehn, J.-M., Grid-type metal ion architectures: Functional metallosupramolecular arrays. *Angew. Chem. Int. Ed.* **2004**, *43* (28), 3644-3662; (b) Fujita, M.; Tominaga, M.; Hori, A.; Therrien, B., Coordination assemblies from a Pd(II)-cornered square complex. *Acc. Chem. Res.* **2005**, *38* (4), 369-378; (c) Chakrabarty, R.; Mukherjee, P. S.; Stang, P. J., Supramolecular coordination: Self-assembly of finite two- and three-dimensional ensembles. *Chem. Rev.* **2011**, *111* (11), 6810-6918; (d) Han, M.; Engelhard, D. M.; Clever, G. H., Self-assembled coordination cages based on banana-shaped ligands. *Chem. Soc. Rev.* **2014**, *43* (6), 1848-1860; (e) Chen, L.-J.; Yang, H.-B.; Shionoya, M., Chiral metallosupramolecular architectures. *Chem. Soc. Rev.* **2017**, *46* (9), 2555-2576; (f) Rizzuto, F. J.; von Krbeke, L. K. S.; Nitschke, J. R., Strategies for binding multiple guests in metal-organic cages. *Nat. Rev. Chem.* **2019**, *3* (4), 204-222.
- (2). (a) Sun, S.-S.; Lees, A. J., Transition metal based supramolecular systems: synthesis, photophysics, photochemistry and their potential applications as luminescent anion chemosensors. *Coord. Chem. Rev.* **2002**, *230* (1), 171-192; (b) Thanasekaran, P.; Liao, R.-T.; Liu, Y.-H.; Rajendran, T.; Rajagopal, S.; Lu, K.-L., Metal-containing molecular rectangles: synthesis and photophysical properties. *Coord. Chem. Rev.* **2005**, *249* (9), 1085-1110; (c) Cook, T. R.; Vajpayee, V.; Lee, M. H.; Stang, P. J.; Chi, K.-W., Biomedical and biochemical applications of self-assembled metallacycles and metallacages. *Acc. Chem. Res.* **2013**, *46* (11), 2464-2474; (d) Zhang, D.; Ronson, T. K.; Nitschke, J. R., Functional capsules via subcomponent self-assembly. *Acc. Chem. Res.* **2018**, *51* (10), 2423-2436; (e) Goswami, A.; Saha, S.; Biswas, P. K.; Schmittel, M., (Nano)mechanical motion triggered by metal coordination: From functional devices to networked multicomponent catalytic machinery. *Chem. Rev.* **2020**, *120* (1), 125-199.
- (3). (a) Neelakandan, P. P.; Jiménez, A.; Nitschke, J. R., Fluorophore incorporation allows nanomolar guest sensing and white-light

emission in M_4L_6 cage complexes. *Chem. Sci.* **2014**, *5* (3), 908-915; (b) Liu, C.-L.; Zhang, R.-L.; Lin, C.-S.; Zhou, L.-P.; Cai, L.-X.; Kong, J.-T.; Yang, S.-Q.; Han, K.-L.; Sun, Q.-F., Intraligand charge transfer sensitization on self-assembled europium tetrahedral cage leads to dual-selective luminescent sensing toward anion and cation. *J. Am. Chem. Soc.* **2017**, *139* (36), 12474-12479; (c) Zhou, Z.; Chen, D. G.; Saha, M. L.; Wang, H.; Li, X.; Chou, P. T.; Stang, P. J., Designed conformation and fluorescence properties of self-assembled phenazine-cored platinum(II) metallacycles. *J. Am. Chem. Soc.* **2019**, *141* (13), 5535-5543; (d) Zhang, Z.; Zhao, Z.; Wu, L.; Lu, S.; Ling, S.; Li, G.; Xu, L.; Ma, L.; Hou, Y.; Wang, X.; Li, X.; He, G.; Wang, K.; Zou, B.; Zhang, M., Emissive platinum(II) cages with reverse fluorescence resonance energy transfer for multiple sensing. *J. Am. Chem. Soc.* **2020**, *142* (5), 2592-2600.

(4). (a) Wu, K.; Li, K.; Hou, Y.-J.; Pan, M.; Zhang, L.-Y.; Chen, L.; Su, C.-Y., Homochiral D₄-symmetric metal-organic cages from stereogenic Ru(II) metalloligands for effective enantioseparation of atropisomeric molecules. *Nat. Commun.* **2016**, *7* (1), 10487; (b) Guo, J.; Fan, Y. Z.; Lu, Y. L.; Zheng, S. P.; Su, C. Y., Visible-light photocatalysis of asymmetric [2+2] cycloaddition in cage-confined nanospace merging chirality with triplet-state photosensitization. *Angew. Chem. Int. Ed.* **2020**, *132* (22), 8739-8747.

(5). (a) Zhang, M.; Li, S.; Yan, X.; Zhou, Z.; Saha, M. L.; Wang, Y.-C.; Stang, P. J., Fluorescent metallacycle-cored polymers via covalent linkage and their use as contrast agents for cell imaging. *Proc. Natl. Acad. Sci. USA* **2016**, *113* (40), 11100; (b) Zhou, J.; Zhang, Y.; Yu, G.; Crowley, M. R.; Fulong, C. R. P.; Friedman, A. E.; Sengupta, S.; Sun, J.; Li, Q.; Huang, F.; Cook, T. R., Highly emissive self-assembled BODIPY-platinum supramolecular triangles. *J. Am. Chem. Soc.* **2018**, *140* (24), 7730-7736; (c) Burke, B. P.; Grantham, W.; Burke, M. J.; Nichol, G. S.; Roberts, D.; Renard, I.; Hargreaves, R.; Cawthorne, C.; Archibald, S. J.; Lusby, P. J., Visualizing kinetically robust Co_4L_6 assemblies *in vivo*: spect imaging of the encapsulated [^{99m}Tc]TcO₄⁻ anion. *J. Am. Chem. Soc.* **2018**, *140* (49), 16877-16881; (d) Wu, L.; Ishigaki, Y.; Hu, Y.; Sugimoto, K.; Zeng, W.; Harimoto, T.; Sun, Y.; He, J.; Suzuki, T.; Jiang, X.; Chen, H.-Y.; Ye, D., H₂S-activatable near-infrared afterglow luminescent probes for sensitive molecular imaging *in vivo*. *Nat. Commun.* **2020**, *11* (1), 446; (e) Yu, G.; Cook, T. R.; Li, Y.; Yan, X.; Wu, D.; Shao, L.; Shen, J.; Tang, G.; Huang, F.; Chen, X.; Stang, P. J., Tetraphenylethene-based highly emissive metallacage as a component of theranostic supramolecular nanoparticles. *Proc. Natl. Acad. Sci. USA* **2016**, *113* (48), 13720.

(6). (a) Chepelin, O.; Ujma, J.; Wu, X.; Slawin, A. M. Z.; Pitak, M. B.; Coles, S. J.; Michel, J.; Jones, A. C.; Barran, P. E.; Lusby, P. J., Luminescent, enantiopure, phenylatopyridine iridium-based coordination capsules. *J. Am. Chem. Soc.* **2012**, *134* (47), 19334-19337; (b) Kaloudi-Chantzea, A.; Karakostas, N.; Pitterl, F.; Raptoulou, C. P.; Glezos, N.; Pistolis, G., Efficient supramolecular synthesis of a robust circular light-harvesting Bodipy-dye based array. *Chem. Commun.* **2012**, (100), 12213-12215.

(7). (a) Yu, G.; Yu, S.; Saha, M. L.; Zhou, J.; Cook, T. R.; Yung, B. C.; Chen, J.; Mao, Z.; Zhang, F.; Zhou, Z.; Liu, Y.; Shao, L.; Wang, S.; Gao, C.; Huang, F.; Stang, P. J.; Chen, X., A discrete organoplatinum(II) metallacage as a multimodality theranostic platform for cancer photochemotherapy. *Nat. Commun.* **2018**, *9* (1), 4335; (b) Qin, Y.; Chen, L.-J.; Dong, F.; Jiang, S.-T.; Yin, G.-Q.; Li, X.; Tian, Y.; Yang, H.-B., Light-controlled generation of singlet oxygen within a discrete dual-stage metallacycle for cancer therapy. *J. Am. Chem. Soc.* **2019**, *141* (22), 8943-8950; (c) Zhou, Z.; Liu, J.; Huang, J.; Rees, T. W.; Wang, Y.; Wang, H.; Li, X.; Chao, H.; Stang, P. J., A self-assembled Ru-Pt metallacage as a lysosome-targeting photosensitizer for 2-photon photodynamic therapy. *Proc. Natl. Acad. Sci. USA* **2019**, *116* (4), 20296.

(8). (a) Saha, M. L.; Yan, X.; Stang, P. J., Photophysical properties of organoplatinum(II) compounds and derived self-assembled metallacycles and metallacages: Fluorescence and its applications. *Acc. Chem. Res.* **2016**, *49* (11), 2527-2539; (b) Kitchen, J. A., Lanthanide-based self-assemblies of 2,6-pyridyldicarboxamide ligands: Recent advances and applications as next-generation luminescent and magnetic materials. *Coord. Chem. Rev.* **2017**, *340*, 232-246; (c) Xuan, W.; Zhang, M.; Liu, Y.; Chen, Z.; Cui, Y., A chiral quadruple-stranded helicate cage for enantioselective recognition and separation. *J. Am. Chem. Soc.* **2012**, *134* (16), 6904-6907; (d) Lewis, J. E. M.; Elliott, A. B. S.; McAdam, C. J.; Gordon, K. C.; Crowley, J. D., 'Click' to functionalise: synthesis, characterisation and enhancement of the physical properties of a series of exo- and endo-functionalised Pd₂L₄ nanocages. *Chem. Sci.* **2014**, *5* (5), 1833-1843; (e) Dalton, D. M.; Ellis, S. R.; Nichols, E. M.; Mathies, R. A.; Toste, F. D.; Bergman, R. G.; Raymond, K. N., Supramolecular Ga₄L₆¹²⁻ cage photosensitizes 1,3-rearrangement of encapsulated guest via photoinduced electron transfer. *J. Am. Chem. Soc.* **2015**, *137* (32), 10128-10131; (f) Yamashina, M.; Sartin, M. M.; Sei, Y.; Akita, M.; Takeuchi, S.; Tahara, T.; Yoshizawa, M., Preparation of highly fluorescent host-guest complexes with tunable color upon encapsulation. *J. Am. Chem. Soc.* **2015**, *137* (29), 9266-9269; (g) Rota Martir, D.; Zysman-Colman, E., Photoactive supramolecular cages incorporating Ru(II) and Ir(III) metal complexes. *Chem. Commun.* **2019**, (2), 139-158; (h) Hu, Y. X.; Hao, X.; Xu, L.; Xie, X.; Xiong, B.; Hu, Z.; Sun, H.; Yin, G. Q.; Li, X.; Peng, H.; Yang, H. B., Construction of supramolecular liquid-crystalline metallacycles for holographic storage of colored images. *J. Am. Chem. Soc.* **2020**, *142* (13), 6285-6294; (i) Chen, L.; Chen, C.; Sun, Y.; Lu, S.; Huo, H.; Tan, T.; Li, A.; Li, X.; Ungar, G.; Liu, F.; Zhang, M., Luminescent metallacycle-cored liquid crystals induced by metal coordination. *Angew. Chem. Int. Ed.* **2020**, *132* (25), 10229-10236; (j) Bogie, P. M.; Miller, T. F.; Hooley, R. J., Synthesis and applications of endohedrally functionalized metal-ligand cage complexes. *Isr. J. Chem.* **2019**, *59* (3-4), 130-139; (k) Samanta, S. K.; Isaacs, L., Biomedical applications of metal organic polygons and polyhedra (MOPs). *Coord. Chem. Rev.* **2020**, *410*, 213181.

(9). (a) Gao, G.-F.; Li, M.; Zhan, S.-Z.; Lv, Z.; Chen, G.-h.; Li, D., Confined metallophilicity within a coordination prism. *Chem. Eur. J.* **2011**, *17* (15), 4113-4117; (b) Li, X.-Z.; Zhou, L.-P.; Yan, L.-L.; Yuan, D.-Q.; Lin, C.-S.; Sun, Q.-F., Evolution of luminescent supramolecular lanthanide M_{2n}L_{3n} complexes from helicates and tetrahedra to cubes. *J. Am. Chem. Soc.* **2017**, *139* (24), 8237-8244.

(10). Rota Martir, D.; Escudero, D.; Jacquemin, D.; Cordes, D. B.; Slawin, A. M. Z.; Fruchtl, H. A.; Warriner, S. L.; Zysman-Colman, E., Homochiral emissive Λ₈- and Δ₈-[Ir₈Pd₄]¹⁶⁺ supramolecular cages. *Chem. Eur. J.* **2017**, *23* (57), 14358-14366.

(11). (a) Ono, K.; Klosterman, J. K.; Yoshizawa, M.; Sekiguchi, K.; Tahara, T.; Fujita, M., ON/OFF red emission from azaporphine in a coordination cage in water. *J. Am. Chem. Soc.* **2009**, *131* (35), 12526-12527; (b) August, D. P.; Nichol, G. S.; Lusby, P. J., Maximizing coordination capsule-guest polar interactions in apolar solvents reveals significant binding. *Angew. Chem. Int. Ed.* **2016**, *55* (48), 15022-15026; (c) Taylor, C. G.; Piper, J. R.; Ward, M. D., Binding of chemical warfare agent simulants as guests in a coordination cage: contributions to binding and a fluorescence-based response. *Chem. Commun.* **2016**, *52* (37), 6225-6228.

(12). (a) Yan, X.; Wang, H.; Hauke, C. E.; Cook, T. R.; Wang, M.; Saha, M. L.; Zhou, Z.; Zhang, M.; Li, X.; Huang, F.; Stang, P. J., A suite of tetraphenylethylene-based discrete organoplatinum(II) metallacycles: controllable structure and stoichiometry, aggregation-induced emission, and nitroaromatics sensing. *J. Am. Chem. Soc.* **2015**, *137* (48), 15276-15286; (b) Yan, X.; Cook, T. R.; Wang, P.; Huang, F.; Stang, P. J., Highly emissive platinum(II) metallacages. *Nat. Chem.* **2015**, *7* (4), 342-348; (c) Lu, C.; Zhang, M.; Tang, D.; Yan, X.; Zhang, Z.; Zhou, Z.; Song, B.; Wang, H.; Li, X.; Yin, S.; Sepehrpour, H.; Stang, P. J., Fluorescent metallacage-core supramolecular polymer gel formed by orthogonal metal coordination and host-guest interactions. *J. Am. Chem. Soc.* **2018**, *140* (24), 7674-7680; (d) Dong, J.; Pan, Y.; Wang, H.; Yang, K.; Liu, L.; Qiao, Z.; Di Yuan, Y.; Peh, S. B.; Zhang, J.; Shi, L.; Liang, H.; Han, Y.; Li, X.; Jiang, J.; Liu, B.; Zhao, D., Self-assembly of highly stable zirconium(IV) coordination cages with aggregation induced emission

- molecular rotors for live-cell imaging. *Angew. Chem. Int. Ed.* **2019**, 10.1002/anie.201915199; (e) Dong, J.; Pan, Y.; Wang, H.; Yang, K.; Liu, L.; Qiao, Z.; Yuan, Y. D.; Peh, S. B.; Zhang, J.; Shi, L.; Liang, H.; Han, Y.; Li, X.; Jiang, J.; Liu, B.; Zhao, D., Self-assembly of highly stable zirconium(IV) coordination cages with aggregation induced emission molecular rotors for live-cell imaging. *Angew. Chem. Int. Ed.* **2020**, 59 (25), 10151-10159.
- (13). (a) Zhang, M.; Saha, M. L.; Wang, M.; Zhou, Z.; Song, B.; Lu, C.; Yan, X.; Li, X.; Huang, F.; Yin, S.; Stang, P. J., Multicomponent platinum(II) cages with tunable emission and amino acid sensing. *J. Am. Chem. Soc.* **2017**, 139 (14), 5067-5074; (b) Musser, A. J.; Neelakandan, P. P.; Richter, J. M.; Mori, H.; Friend, R. H.; Nitschke, J. R., Excitation energy delocalization and transfer to guests within M₄L₆ cage frameworks. *J. Am. Chem. Soc.* **2017**, 139 (34), 12050-12059; (c) Käseborn, M.; Holstein, J. J.; Clever, G. H.; Lützen, A., A rotaxane-like cage-in-ring structural motif for a metallocupramolecular Pd₆L₁₂ aggregate. *Angew. Chem. Int. Ed.* **2018**, 57 (37), 12171-12175.
- (14). (a) Wang, J.; He, C.; Wu, P.; Wang, J.; Duan, C., An amide-containing metal-organic tetrahedron responding to a spin-trapping reaction in a fluorescent enhancement manner for biological imaging of NO in living cells. *J. Am. Chem. Soc.* **2011**, 133 (32), 12402-12405; (b) Zhu, J. L.; Xu, L.; Ren, Y. Y.; Zhang, Y.; Liu, X.; Yin, G. Q.; Sun, B.; Cao, X.; Chen, Z.; Zhao, X. L.; Tan, H.; Chen, J.; Li, X.; Yang, H. B., Switchable organoplatinum metallacycles with high quantum yields and tunable fluorescence wavelengths. *Nat. Commun.* **2019**, 10 (1), 4285.
- (15). Chang, X.; Zhou, Z.; Shang, C.; Wang, G.; Wang, Z.; Qi, Y.; Li, Z. Y.; Wang, H.; Cao, L.; Li, X.; Fang, Y.; Stang, P. J., Coordination-driven self-assembled metallacycles incorporating pyrene: Fluorescence mutability, tunability, and aromatic amine sensing. *J. Am. Chem. Soc.* **2019**, 141 (4), 1757-1765.
- (16). (a) Mahata, K.; Frischmann, P. D.; Würthner, F., Giant electroactive M₄L₆ tetrahedral host self-assembled with Fe(II) vertices and perylene bisimide dye edges. *J. Am. Chem. Soc.* **2013**, 135 (41), 15656-15661; (b) Frischmann, P. D.; Kunz, V.; Würthner, F., Bright fluorescence and host-guest sensing with a nanoscale M₄L₆ tetrahedron accessed by self-assembly of zinc-imine chelate vertices and perylene bisimide edges. *Angew. Chem. Int. Ed.* **2015**, 54 (25), 7285-7289.
- (17). (a) Li, K.; Zhang, L.-Y.; Yan, C.; Wei, S.-C.; Pan, M.; Zhang, L.; Su, C.-Y., Stepwise assembly of Pd₆(RuL₃)₈ nanoscale rhombododecahedral metal-organic cages via metalloligand strategy for guest trapping and protection. *J. Am. Chem. Soc.* **2014**, 136 (12), 4456-4459; (b) Chen, S.; Li, K.; Zhao, F.; Zhang, L.; Pan, M.; Fan, Y.-Z.; Guo, J.; Shi, J.; Su, C.-Y., A metal-organic cage incorporating multiple light harvesting and catalytic centres for photochemical hydrogen production. *Nat. Commun.* **2016**, 7 (1), 13169.
- (18). (a) Stomeo, F.; Linceneau, C.; Leonard, J. P.; O'Brien, J. E.; Peacock, R. D.; McCoy, C. P.; Gunnlaugsson, T., Metal-directed synthesis of enantiomerically pure dimetallic lanthanide luminescent triple-stranded helicates. *J. Am. Chem. Soc.* **2009**, 131 (28), 9636-9637; (b) Yeung, C.-T.; Chan, W. T. K.; Yan, S.-C.; Yu, K.-L.; Yim, K.-H.; Wong, W.-T.; Law, G.-L., Lanthanide supramolecular helical diastereoselective breaking induced by point chirality: mixture or P-helix, M-helix. *Chem. Commun.* **2015**, (3), 592-595; (c) Yan, L.-L.; Tan, C.-H.; Zhang, G.-L.; Zhou, L.-P.; Bünzli, J.-C.; Sun, Q.-F., Stereocontrolled self-assembly and self-sorting of luminescent europium tetrahedral cages. *J. Am. Chem. Soc.* **2015**, 137 (26), 8550-8555; (d) Guo, X.-Q.; Zhou, L.-P.; Cai, L.-X.; Sun, Q.-F., Self-assembled bright luminescent lanthanide-organic polyhedra for ratiometric temperature sensing. *Chem. Eur. J.* **2018**, 24 (27), 6936-6940.
- (19). Schmittel, M.; Shu, Q.; Cinar, M. E., Tuning the wavelength of electrochemiluminescence by anodic potential: a design using non-Kekulé-structured iridium-ruthenium luminophores. *Dalton Trans.* **2012**, 41 (20), 6064-6068.
- (20). (a) Goeb, S.; Prusakova, V.; Wang, X.; Vézinat, A.; Sallé, M.; Castellano, F. N., Phosphorescent self-assembled Pt^{II} tetranuclear metallocycles. *Chem. Commun.* **2011**, (15), 4397-4399; (b) Pollock, J. B.; Schneider, G. L.; Cook, T. R.; Davies, A. S.; Stang, P. J., Tunable visible light emission of self-assembled rhomboidal metallocycles. *J. Am. Chem. Soc.* **2013**, 135 (37), 13676-13679; (c) Zhang, Y.; Fulong, C. R. P.; Hauke, C. E.; Crawley, M. R.; Friedman, A. E.; Cook, T. R., Photophysical enhancement of triplet emitters by coordination-driven self-assembly. *Chem. Eur. J.* **2017**, 23 (19), 4532-4536; (d) Zhou, Z.; Hauke, C. E.; Song, B.; Li, X.; Stang, P. J.; Cook, T. R., Understanding the effects of coordination and self-assembly on an emissive phenothiazine. *J. Am. Chem. Soc.* **2019**, 141 (8), 3717-3722; (e) Bhattacharyya, S.; Chowdhury, A.; Saha, R.; Mukherjee, P. S., Multifunctional self-assembled macrocycles with enhanced emission and reversible photochromic behavior. *Inorg. Chem.* **2019**, 58 (6), 3968-3981; (f) Pollock, J. B.; Cook, T. R.; Schneider, G. L.; Lutterman, D. A.; Davies, A. S.; Stang, P. J., Photophysical properties of endohedral amine-functionalized bis(phosphine) Pt(II) complexes as models for emissive metallocycles. *Inorg. Chem.* **2013**, 52 (16), 9254-9265; (g) Acharyya, K.; Bhattacharyya, S.; Sepehrpour, H.; Chakraborty, S.; Lu, S.; Shi, B.; Li, X.; Mukherjee, P. S.; Stang, P. J., Self-assembled fluorescent Pt(II) metallocycles as artificial light-harvesting systems. *J. Am. Chem. Soc.* **2019**, 141 (37), 14565-14569.
- (21). (a) Jiang, X.-F.; Hau, F. K.-W.; Sun, Q.-F.; Yu, S.-Y.; Yam, V. W.-W., From {AuI...AuI}-coupled cages to the cage-built 2-D {AuI...AuI} arrays: AuI...AuI bonding interaction driven self-assembly and their AgI sensing and photo-switchable behavior. *J. Am. Chem. Soc.* **2014**, 136 (31), 10921-10929; (b) Li, Y.; An, Y.-Y.; Fan, J.-Z.; Liu, X.-X.; Li, X.; Hahn, F. E.; Wang, Y.-Y.; Han, Y.-F., Strategy for the construction of diverse poly-NHC-derived assemblies and their photoinduced transformations. *Angew. Chem. Int. Ed.* **2019**, 59 (25), 10073-10080; (c) Sun, L.-Y.; Feng, T.; Das, R.; Hahn, F. E.; Han, Y.-F., Synthesis, characterization, and properties of tetraphenylethylene-based tetrakis-NHC ligands and their metal complexes. *Chem. Eur. J.* **2019**, 25 (41), 9764-9770.
- (22). (a) Wu, S.-Y.; Guo, X.-Q.; Zhou, L.-P.; Sun, Q.-F., Fine-tuned visible and near-infrared luminescence on self-assembled lanthanide-organic tetrahedral cages with triazole-based chelates. *Inorg. Chem.* **2019**, 58 (10), 7091-7098; (b) Zhang, Y.; Crawley, M. R.; Hauke, C. E.; Friedman, A. E.; Cook, T. R., Phosphorescent decanuclear bimetallic Pt₆M₄ (M = Zn, Fe) tetrahedral cages. *Inorg. Chem.* **2017**, 56 (8), 4258-4262; (c) Zhang, Y.; Cox, J. M.; Friedman, A. E.; Benedict, J. B.; Cook, T. R., Phosphorescent organoplatinum(II) D₂A₂ metallocycles: synthesis, self-assembly, and photophysical properties. *J. Coord. Chem.* **2016**, 69 (11-13), 1914-1923.
- (23). (a) Chakraborty, S.; Newkome, G. R., Terpyridine-based metallocupramolecular constructs: tailored monomers to precise 2D-motifs and 3D-metallocages. *Chem. Soc. Rev.* **2018**, 47 (11), 3991-4016; (b) Newkome, G. R.; Wang, P. S.; Moorefield, C. N.; Cho, T. J.; Mohapatra, P. P.; Li, S. N.; Hwang, S. H.; Lukyanova, O.; Echegoyen, L.; Palagallo, J. A.; Iancu, V.; Hla, S. W., Nanoassembly of a fractal polymer: A molecular "Sierpinski hexagonal gasket". *Science* **2006**, 312 (5781), 1782-1785; (c) Fu, J.-H.; Lee, Y.-H.; He, Y.-J.; Chan, Y.-T., Facile self-assembly of metallo-supramolecular ring-in-ring and spiderweb structures using multivalent terpyridine ligands. *Angew. Chem. Int. Ed.* **2015**, 54 (21), 6231-6235; (d) Xie, T. Z.; Guo, K.; Guo, Z. H.; Gao, W. Y.; Wojtas, L.; Ning, G. H.; Huang, M. J.; Lu, X. C.; Li, J. Y.; Liao, S. Y.; Chen, Y. S.; Moorefield, C. N.; Saunders, M. J.; Cheng, S. Z. D.; Wesdemiotis, C.; Newkome, G. R., Precise molecular fission and fusion: Quantitative self-assembly and chemistry of a metallo-cuboctahedron. *Angew. Chem. Int. Ed.* **2015**, 54 (32), 9224-9229; (e) Li, Y.; Jiang, Z.; Wang, M.; Yuan, J.; Liu, D.; Yang, X.; Chen, M.; Yan, J.; Li, X.; Wang, P., Giant, hollow 2D metalloarchitecture: Stepwise self-assembly of a hexagonal supramolecular nut. *J. Am. Chem. Soc.* **2016**, 138 (31), 10041-10046; (f) Wang, S.-Y.; Fu, J.-H.; Liang, Y.-P.; He, Y.-J.; Chen, Y.-S.; Chan, Y.-T., Metallo-supramolecular self-assembly of a multicomponent

ditrignon based on complementary terpyridine ligand pairing. *J. Am. Chem. Soc.* **2016**, *138* (11), 3651-3654; (g) Jiang, Z.; Li, Y.; Wang, M.; Song, B.; Wang, K.; Sun, M.; Liu, D.; Li, X.; Yuan, J.; Chen, M.; Guo, Y.; Yang, X.; Zhang, T.; Moorefield, C. N.; Newkome, G. R.; Xu, B.; Li, X.; Wang, P., Self-assembly of a supramolecular hexagram and a supramolecular pentagram. *Nat. Commun.* **2017**, *8* (1), 15476; (h) Wang, H.; Qian, X.; Wang, K.; Su, M.; Haoyang, W. W.; Jiang, X.; Brzozowski, R.; Wang, M.; Gao, X.; Li, Y.; Xu, B.; Eswara, P.; Hao, X. Q.; Gong, W.; Hou, J. L.; Cai, J.; Li, X., Supramolecular Kandinsky circles with high antibacterial activity. *Nat. Commun.* **2018**, *9* (1), 1815; (i) Liu, D.; Chen, M.; Li, Y.; Shen, Y.; Huang, J.; Yang, X.; Jiang, Z.; Li, X.; Newkome, G. R.; Wang, P., Vertical assembly of giant double- and triple-decker spoked wheel supramolecular structures. *Angew. Chem. Int. Ed.* **2018**, *57* (43), 14116-14120; (j) Chen, Y.-S.; Solel, E.; Huang, Y.-F.; Wang, C.-L.; Tu, T.-H.; Keinan, E.; Chan, Y.-T., Chemical mimicry of viral capsid self-assembly via corannulene-based pentatopic tectons. *Nat. Commun.* **2019**, *10* (1), 3443; (k) Zhang, Z.; Li, Y.; Song, B.; Zhang, Y.; Jiang, X.; Wang, M.; Trumbleson, R.; Liu, C.; Wang, P.; Hao, X.-Q.; Rojas, T.; Ngo, A. T.; Sessler, J. L.; Newkome, G. R.; Hla, S. W.; Li, X., Intra- and intermolecular self-assembly of a 20-nm-wide supramolecular hexagonal grid. *Nat. Chem.* **2020**, *12*, 468-474.

(24). (a) Constable, E. C., 2,2':6',2''-Terpyridines: From chemical obscurity to common supramolecular motifs. *Chem. Soc. Rev.* **2007**, *36* (2), 246-253; (b) Wild, A.; Winter, A.; Schlütter, F.; Schubert, U. S., Advances in the field of π -conjugated 2,2':6',2''-terpyridines. *Chem. Soc. Rev.* **2011**, *40* (3), 1459-1511.

(25). (a) Chen, X. G.; Ding, Y. Q.; Cheng, Y. X.; Wang, L. X., Synthesis, spectroscopy and electroluminescence of cadmium(II) polypyridyl complexes. *Synth. Met.* **2010**, *160* (7-8), 625-630; (b) Wang, J. L.; Li, X. P.; Lu, X. C.; Chan, Y. T.; Moorefield, C. N.; Wesdemiotis, C.; Newkome, G. R., Dendron-functionalized bis(terpyridine)-iron(II) or -cadmium(II) metallomacrocycles: Synthesis, traveling-wave ion-mobility mass spectrometry, and photophysical properties. *Chem. Eur. J.* **2011**, *17* (17), 4830-4838; (c) Schultz, A.; Cao, Y.; Huang, M. J.; Cheng, S. Z. D.; Li, X. P.; Moorefield, C. N.; Wesdemiotis, C.; Newkome, G. R., Stable, trinuclear Zn(II)- and Cd(II)-metallocycles: TWIM-MS, photophysical properties, and nanofiber formation. *Dalton Trans.* **2012**, *41* (38), 11573-11575; (d) Yin, G. Q.; Wang, H.; Wang, X. Q.; Song, B.; Chen, L. J.; Wang, L.; Hao, X. Q.; Yang, H. B.; Li, X., Self-assembly of emissive supramolecular rosettes with increasing complexity using multitopic terpyridine ligands. *Nat. Commun.* **2018**, *9* (1), 567; (e) Liu, D.; Chen, M.; Li, K.; Li, Z.; Huang, J.; Wang, J.; Jiang, Z.; Zhang, Z.; Xie, T.; Newkome, G. R.; Wang, P., Giant truncated metallo-tetrahedron with unexpected supramolecular aggregation induced emission enhancement. *J. Am. Chem. Soc.* **2020**, *142* (17), 7987-7994.

(26). (a) Luo, J.; Xie, Z.; Lam, J. W. Y.; Cheng, L.; Chen, H.; Qiu, C.; Kwok, H. S.; Zhan, X.; Liu, Y.; Zhu, D.; Tang, B. Z., Aggregation-induced emission of 1-methyl-1,2,3,4,5-pentaphenylsilole. *Chem. Commun.* **2001**, (18), 1740-1741; (b) Hong, Y.; Lam, J. W. Y.; Tang, B. Z., Aggregation-induced emission: phenomenon, mechanism and applications. *Chem. Commun.* **2009**, (29), 4332-4353; (c) Hong, Y.; Lam, J. W. Y.; Tang, B. Z., Aggregation-induced emission. *Chem. Soc. Rev.* **2011**, *40* (11), 5361-5388; (d) Hu, R.; Leung, N. L. C.; Tang, B. Z., AIE macromolecules: syntheses, structures and functionalities. *Chem. Soc. Rev.* **2014**, *43* (13), 4494-4562; (e) Mei, J.; Leung, N. L. C.; Kwok, R. T. K.; Lam, J. W. Y.; Tang, B. Z., Aggregation-induced emission: Together we shine, united we soar! *Chem. Rev.* **2015**, *115* (21), 11718-11940; (f) Chowdhury, A.; Howlader, P.; Mukherjee, P. S., Aggregation-induced emission of platinum(II) metallacycles and their ability to detect nitroaromatics. *Chem. Eur. J.* **2016**, *22* (22), 7468-7478; (g) Das, P.; Kumar, A.; Chowdhury, A.; Mukherjee, P. S., Aggregation-induced emission and white luminescence from a combination of π -conjugated donor-acceptor organic luminogens. *ACS Omega* **2018**, *3* (10), 13757-13771; (h) Dong, J.; Li, X.; Zhang, K.; Di Yuan, Y.; Wang, Y.; Zhai, L.; Liu, G.; Yuan, D.; Jiang, J.; Zhao, D., Confinement of aggregation-induced emission molecular rotors in ultrathin two-dimensional porous organic nanosheets for enhanced molecular recognition. *J. Am. Chem. Soc.* **2018**, *140* (11), 4035-4046.

(27). (a) Ott, C.; Ulbricht, C.; Hoogenboom, R.; Schubert, U. S., Metallo-supramolecular materials based on amine-grafting onto polypentafluorostyrene. *Macromol. Rapid Commun.* **2012**, *33* (6-7), 556-561; (b) Fermi, A.; Bergamini, G.; Roy, M.; Gingras, M.; Ceroni, P., Turn-on phosphorescence by metal coordination to a multivalent terpyridine ligand: A new paradigm for luminescent sensors. *J. Am. Chem. Soc.* **2014**, *136* (17), 6395-6400.

(28). (a) Cummings, S. D., Platinum complexes of terpyridine: Synthesis, structure and reactivity. *Coord. Chem. Rev.* **2009**, *253* (3), 449-478; (b) Yam, V. W. W.; Au, V. K. M.; Leung, S. Y. L., Light-emitting self-assembled materials based on d(8) and d(10) transition metal complexes. *Chem. Rev.* **2015**, *115* (15), 7589-7728; (c) Chowdhury, A.; Howlader, P.; Mukherjee, P. S., Mechano-fluorochromic Pt^{II} luminogen and its cysteine recognition. *Chem. Eur. J.* **2016**, *22* (4), 1424-1434.

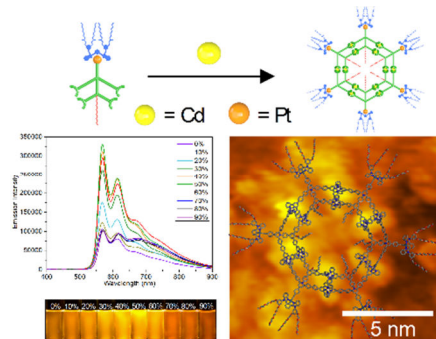
(29). (a) Castellano, F. N.; Pomestchenko, I. E.; Shikhova, E.; Hua, F.; Muro, M. L.; Rajapakse, N., Photophysics in bipyridyl and terpyridyl platinum(II) acetylides. *Coord. Chem. Rev.* **2006**, *250* (13), 1819-1828; (b) Wong, W.-Y.; Ho, C.-L., Organometallic photovoltaics: A new and versatile approach for harvesting solar energy using conjugated polymetallaynes. *Acc. Chem. Res.* **2010**, *43* (9), 1246-1256; (c) Chan, A. K.-W.; Yam, V. W.-W., Precise modulation of molecular building blocks from tweezers to rectangles for recognition and stimuli-responsive processes. *Acc. Chem. Res.* **2018**, *51* (12), 3041-3051; (d) Cardolaccia, T.; Li, Y.; Schanze, K. S., Phosphorescent platinum acetylide organogelators. *J. Am. Chem. Soc.* **2008**, *130* (8), 2535-2545.

(30). (a) Yuen, M.-Y.; Roy, V. A. L.; Lu, W.; Kui, S. C. F.; Tong, G. S. M.; So, M.-H.; Chui, S. S.-Y.; Muccini, M.; Ning, J. Q.; Xu, S. J.; Che, C.-M., Semiconducting and electroluminescent nanowires self-assembled from organoplatinum(II) complexes. *Angew. Chem. Int. Ed.* **2008**, *47* (51), 9895-9899; (b) Strasser, C. A.; Chien, C.-H.; Galvez Lopez, M. D.; Kourkoulos, D.; Hertel, D.; Meerholz, K.; De Cola, L., Switching on luminescence by the self-assembly of a platinum(II) complex into gelating nanofibers and electroluminescent films. *Angew. Chem. Int. Ed.* **2011**, *50* (4), 946-950; (c) Leung, S. Y. L.; Wong, K. M. C.; Yam, V. W. W., Self-assembly of alkynylplatinum(II) terpyridine amphiphiles into nanostructures via steric control and metal-metal interactions. *Proc. Natl. Acad. Sci. USA* **2016**, *113* (11), 2845-2850; (d) Li, Y. G.; Chen, L.; Ai, Y. Y.; Hong, E. Y. H.; Chan, A. K. W.; Yam, V. W. W., Supramolecular self-assembly and dual-switch vapochromic, vapoluminescent, and resistive memory behaviors of amphiphilic platinum(II) complexes. *J. Am. Chem. Soc.* **2017**, *139* (39), 13858-13866; (e) Chan, M. H. Y.; Leung, S. Y. L.; Yam, V. W. W., Controlling self-assembly mechanisms through rational molecular design in oligo(p-phenyleneethynylene)-containing alkynylplatinum(II) 2,6-bis(n-alkylbenzimidazol-2'-yl)pyridine amphiphiles. *J. Am. Chem. Soc.* **2018**, *140* (24), 7637-7646; (f) Lu, W.; Chen, Y.; Roy, V. A. L.; Chui, S. S.-Y.; Che, C.-M., Supramolecular polymers and chromonic mesophases self-organized from phosphorescent cationic organoplatinum(II) complexes in water. *Angew. Chem. Int. Ed.* **2009**, *48* (41), 7621-7625; (g) Yu-Lut Leung, S.; Wing-Wah Yam, V., Hierarchical helices of helices directed by Pt...Pt and π - π stacking interactions: reciprocal association of multiple helices of dinuclear alkynylplatinum(II) complex with luminescence enhancement behavior. *Chem. Sci.* **2013**, *4* (11), 4228-4234.

(31). (a) Ravotto, L.; Ceroni, P., Aggregation induced phosphorescence of metal complexes: From principles to applications. *Coord. Chem. Rev.* **2017**, *346*, 62-76; (b) You, Y.; Huh, H. S.; Kim, K. S.; Lee, S. W.; Kim, D.; Park, S. Y., Comment on 'aggregation-induced phosphorescent emission (AIPE) of iridium(III) complexes': origin of the enhanced phosphorescence. *Chem. Commun.* **2008**, (34), 3998-4000; (c) Zhao, Q.; Li, L.; Li, F.; Yu, M.; Liu, Z.; Yi, T.;

- Huang, C., Aggregation-induced phosphorescent emission (AIPE) of iridium(III) complexes. *Chem. Commun.* **2008**, (6), 685-687; (d) Liu, S.; Sun, H.; Ma, Y.; Ye, S.; Liu, X.; Zhou, X.; Mou, X.; Wang, L.; Zhao, Q.; Huang, W., Rational design of metallophosphors with tunable aggregation-induced phosphorescent emission and their promising applications in time-resolved luminescence assay and targeted luminescence imaging of cancer cells. *J. Mater. Chem.* **2012**, 22 (41), 22167-22173.
- (32). Fu, H. L. K.; Po, C.; Leung, S. Y. L.; Yam, V. W. W., Self-assembled architectures of alkynylplatinum(II) amphiphiles and their structural optimization: a balance of the interplay among Pt...Pt, pi-pi stacking, and hydrophobic-hydrophobic interactions. *ACS Appl. Mater. Interfaces* **2017**, 9 (3), 2786-2795.
- (33). Chan, Y.-T.; Li, X.; Soler, M.; Wang, J.-L.; Wesdemiotis, C.; Newkome, G. R., Self-assembly and traveling wave ion mobility mass spectrometry analysis of hexacadmium macrocycles. *J. Am. Chem. Soc.* **2009**, 131 (45), 16395-16397.
- (34). (a) Wang, H.; Li, Y.; Yu, H.; Song, B.; Lu, S.; Hao, X.-Q.; Zhang, Y.; Wang, M.; Hla, S.-W.; Li, X., Combining synthesis and self-assembly in one pot to construct complex 2D metallo-supramolecules using terpyridine and pyrylium salts. *J. Am. Chem. Soc.* **2019**, 141 (33), 13187-13195; (b) Li, Z.; Li, Y.; Zhao, Y.; Wang, H.; Zhang, Y.; Song, B.; Li, X.; Lu, S.; Hao, X.-Q.; Hla, S.-W.; Tu, Y.; Li, X., Synthesis of metallopolymers and direct visualization of the single polymer chain. *J. Am. Chem. Soc.* **2020**, 142 (13), 6196-6205.
- (35). Kong, F. K. W.; Tang, M. C.; Wong, Y. C.; Ng, M.; Chan, M. Y.; Yam, V. W. W., Strategy for the realization of efficient solution-processable phosphorescent organic light-emitting devices: Design and synthesis of bipolar alkynylplatinum(II) complexes. *J. Am. Chem. Soc.* **2017**, 139 (18), 6351-6362.
- (36). (a) Wang, K.; Haga, M.-a.; Monjushiro, H.; Akiba, M.; Sasaki, Y., Luminescent langmuir-blodgett films of platinum(II) complex [Pt(L18)Cl](PF₆) (L18 = 2,6-bis(1-octadecylbenzimidazol-2-yl)pyridine). *Inorg. Chem.* **2000**, 39 (18), 4022-4028; (b) Mathew, I.; Sun, W., Photophysics in solution and Langmuir-Blodgett film and vapo-chromic behavior of the Pt(II) 2,6-bis(N-alkylbenzimidazol-2'-yl)pyridine complexes with different alkyl chains and counter anions. *Dalton Trans.* **2010**, 39 (25), 5885-5898.
- (37). (a) Ji, Z.; Azenkeng, A.; Hoffmann, M.; Sun, W., Synthesis and photophysics of 4'-R-2,2';6',2''-terpyridyl (R = Cl, CN, N(CH₃)₂) platinum(II) phenylacetylde complexes. *Dalton Trans.* **2009**, (37), 7725-7733; (b) Shao, P.; Li, Y.; Yi, J.; Pritchett, T. M.; Sun, W., Cyclometalated platinum(II) 6-phenyl-4-(9,9-dihexylfluoren-2-yl)-2,2'-bipyridine complexes: synthesis, photophysics, and nonlinear absorption. *Inorg. Chem.* **2010**, 49 (10), 4507-4517.
- (38). Po, C.; Yam, V. W. W., A metallo-amphiphile with unusual memory behaviour: effect of temperature and structure on the self-assembly of triethylene glycol (TEG)-pendant platinum(II) bzimpy complexes. *Chem. Sci.* **2014**, 5 (12), 4868-4872.
- (39). Au-Yeung, H. L.; Tam, A. Y. Y.; Leung, S. Y. L.; Yam, V. W. W., Supramolecular assembly of platinum-containing polyhedral oligomeric silsesquioxanes: an interplay of intermolecular interactions and a correlation between structural modifications and morphological transformations. *Chem. Sci.* **2017**, 8 (3), 2267-2276.
- (40). (a) Czerwinski, A.; Sobkowski, J., Kinetics of adsorbed "CO₂" oxidation on a platinum electrode. *J. Electroanal. Chem. Interf. Electrochem.* **1975**, 59 (1), 41-46; (b) Ishiji, T.; Takahashi, K.; Kira, A., Amperometric carbon dioxide gas sensor based on electrode reduction of platinum oxide. *Anal. Chem.* **1993**, (65), 2736-2739; (c) Wang, H.; Zhang, L.; Zhou, Y.; Qiao, S.; Liu, X.; Wang, W., Photocatalytic CO₂ reduction over platinum modified hexagonal tungsten oxide: Effects of platinum on forward and back reactions. *Appl. Catal. B* **2020**, 263, 118331.
- (41). (a) Yuan, H.; Tao, J.; Li, N.; Karmakar, A.; Tang, C.; Cai, H.; Pennycook, S. J.; Singh, N.; Zhao, D., On-chip tailorability of capacitive gas sensors integrated with metal-organic framework films. *Angew. Chem. Int. Ed.* **2019**, 58 (40), 14089-14094; (b) Yuan, H.; Li, N.; Linghu, J.; Dong, J.; Wang, Y.; Karmakar, A.; Yuan, J.; Li, M.; Buenconsejo, P. J. S.; Liu, G.; Cai, H.; Pennycook, S. J.; Singh, N.; Zhao, D., Chip-level integration of covalent organic frameworks for trace benzene sensing. *ACS Sensors* **2020**, 5 (5), 1474-1481.
- (42). (a) Che, C.-M.; Chow, C.-F.; Yuen, M.-Y.; Roy, V. A. L.; Lu, W.; Chen, Y.; Chui, S. S.-Y.; Zhu, N., Single microcrystals of organoplatinum(II) complexes with high charge-carrier mobility. *Chem. Sci.* **2011**, 2 (2), 216-220; (b) Kong, F. K. W.; Chan, A. K. W.; Ng, M.; Low, K. H.; Yam, V. W. W., Construction of discrete pentanuclear platinum(II) stacks with extended metal-metal interactions by using phosphorescent platinum(II) tweezers. *Angew. Chem. Int. Ed.* **2017**, 56 (47), 15103-15107.

Table of Contents



A new discrete metallo-supramolecular concentric hexagon functionalized with six alkynylplatinum(II) bzimpy moieties was prepared. With a size larger than 10 nm and molecular weight higher than 26,000 Da, the assembled supramolecule displayed phosphorescent emission at room temperature. Moreover, the supramolecule exhibited enhanced aggregation-induced phosphorescent emission compared to the ligand.